INDC International Nuclear Data Committee

Updating of data for the neutron yields in reactor fuels

for the interest of Nuclear Safeguards

Quincy van den Berg, Stanislav Simakov

Nuclear Data Section,
International Atomic Energy Agency
Vienna, Austria

October 2015

Updating of data for the neutron yields in reactor fuels

for the interest of Nuclear Safeguards

Internship Report of Quincy van den Berg for period 24 Aug - 18 Oct 2015

Quincy van den Berg, Stanislav Simakov

Nuclear Data Section, IAEA

Abstract

We re-evaluated the neutron yield from (α,xn) reactions for actinides embedded in reactor fuel materials. The alpha particles originate from spontaneous α-decay of actinides and subsequently produce neutrons interacting with the light elements in compound materials. This report provides an update of the α-n yields tables released by the Los Alamos National Lab in 1991 for the UO_2, UF_6, PuO_2 and PuF_4 samples containing ^{241}Am, ^{249}Bk, ^{252}Cf, ^{242,244}Cm, ^{237}Np, $^{238-242}$Pu, ^{232}Th and $^{232-236,238}$U isotopes. The latest evaluations of alpha decay, stopping power and neutron production cross sections have been employed in present calculations, the uncertainty ranges were additionally estimated. The results show an agreement with 1991 reference data for neutron yields caused by decaying actinides embedded in oxides UO_2 and PuO_2 within 10%, however 25-50% differences for UF_6 and PuF_4. The main reason for this was found to be the update of the ^{19}F(α,n) reaction cross section, which still need more accurate re-measurement and re-evaluation.

Revision 1 includes modifications made in Figs 2, 3 and 6, partial densities for oxygen isotopes as well as newly calculated yields and ratios in Tables 3, 4 and 5.

Revision 2 includes modifications of Tables 2 - 6.

Contents

1. Introduction

Most alpha particles emitted by heavy isotopes embedded in reactor fuel materials are not detected outside the fuel container as they have an extremely short projected range. They deposit all their kinetic energy within a typical range of under 10 μm and in doing so, they interact with lighter elements in the same fuel material through neutron producing reactions. This work considers a selection of alpha emitters from the actinide series which generally have long decay times. Due to their long-lasting alpha emission, they contribute to a steady neutron production in reactor fuel materials even after the fuel has been depleted.

Each alpha emitting isotope has its own half-life which affects the yield of alpha particles directly, as well as a different radiation emission spectrum. The differences in radiation emission spectrum affect the neutron yield from (α,xn) reactions due to the energy dependent cross sections of said reactions. Therefore, the (α,xn) neutron yield will differ for each alpha emitting isotope that finds potential applications in Safeguards, but is also relevant for the standards concerning radiation safety.

Before the release of this revision, the most recent evaluation for the (α,xn) neutron yield has been carried out by the Los Alamos National Laboratory for the isotopes ^{241}Am, ^{249}Bk, ^{252}Cf, ^{242,244}Cm, ^{237}Np, $^{238-242}$Pu, ^{232}Th and $^{232-236,238}$U and dates back to 1991, see Table 11-3 on page 345 of Report NUREG/CR-5550 [1]. However the (α,n) reaction neutron yields listed there for UO_2 refer to the even older Report published in 1981 [2] and for UF_6 and PuF_4 to several publications appeared from 1974 to 1983.

Since then, new alpha decay data, (α,xn) cross section and α-stopping power evaluations have appeared [3-5]. In addition to the input data being outdated, the 1991 evaluation specifies the uncertainty only for uranium oxide and generally as 10%.

The present revision intends to incorporate the most recent input data as well as quantify the uncertainty in the neutron yield to serve as an update of Table 11-3 of [1].

The following approach was used:
- collection and critical review of the available cross sections for (α,xn) reactions occurring in reactor fuel materials;
- calculation of the stopping power of alpha-particles in fuel materials using the SRIM and ASTAR codes;
- collection and critical review of the alpha decay data from the DDEP and ENSDF databases for the considered isotopes;
- calculation of the (α,xn) neutron yield for the selected isotopes including their uncertainty range in a newly assembled Fortran 90 script.

In this revision, the neutron yield computing method is described as well as the relevant input data. This includes alpha decay data, neutron production cross sections and the stopping power which are compared with experimental data. The Fortran 90 code was validated using experimental thick target neutron yield data on uranium oxide, after that it was used to compute the neutron yield for actinides in reactor fuel materials.

2. Neutron yield equation

The production of neutrons through alpha induced reactions in fuel materials can be treated mathematically as that of alpha particles colliding with a thick target. In this context, a thick target must be thick enough to prevent any alpha particles from escaping, meaning they lose all their kinetic energy within the target. As will be verified later in the subsection on stopping power, this condition is met already for targets exceeding a 50 μm thickness and thus validates this mathematical approach. Thick target yields can also be accurately measured, allowing the experimental verification of the validity of the calculation method used in this report.

The thick target neutron yield of an incident alpha particle with energy E_α can be calculated by formula:

$$Y_n(E_\alpha) = N_T \int_0^{E_\alpha} \sigma_n |S(E)|^{-1} dE, \qquad \text{in units neutrons/α-particle,}$$

where N_T is the atomic density of the target nucleus, σ_n represents the neutron production cross section of the target nucleus and $S(E)$ is the linear stopping power of the reactor fuel material. In order to compute the neutron yield per gram of each isotope of interest, the yield equation must be expanded to sum over all reaction channels:

$$Y_{n,tot} = \frac{\ln 2}{T_{1/2}} \frac{N_{Avo}}{M_{iso}} \sum_{E_\alpha} P(E_\alpha) Y_n(E_\alpha), \qquad \text{in units neutrons/s·g.}$$

In this expression, the summation runs over all reaction channels with energy E_α and probability $P(E_\alpha)$ to compute the average neutron yield per emitted α-particle. The prefactor before the summation represents the alpha yield ($\alpha/s \cdot g$) of the emitting isotope where $T_{1/2}$ denotes the half-life, M_{iso} is the isotope's molar mass and N_{Avo} denotes Avogadro's number, respectively. Finally, a neutron yield per gram of isotope obtained directly links the neutron yield to a certain quantity of each isotope of interest.

In the case of compound targets consisting of different types of target nuclei, their contribution are linearly summed with weights according to the atomic densities. This is the case for oxygen which has three naturally occurring isotopes. The neutron yield resulting from such a target is computed from the weighted average of each target isotope's contribution to the yield.

3. Input data

In order to calculate neutron yields with the equations from the previous section, several types of input data are required. This includes alpha decay data such as the possible decay energies and their respective branching fractions. Secondly, the neutron production cross sections are needed of all elements present in reactor fuel that have a threshold in the alpha energy range. Furthermore, the stopping power is needed to describe how the alpha particles are stopped inside the fuel material.

The data for these quantities are presented in the following sub-sections.

3.1 Alpha-decay data

This work re-evaluates the neutron yield in reactor fuel material as a result of alpha particles emitted through spontaneous α-decay of embedded heavy elements. These elements are [241]Am, [249]Bk, [252]Cf, [242,244]Cm, [237]Np, [238-242]Pu, [232]Th and [232-236,238]U, some of which are extremely long-lived isotopes. Across all elements and alpha decay channels, the alpha-particle energies lie between 3.8 and 6.2 MeV [6].

The isotopes under evaluation emit alpha particles through a total of 246 reaction channels, averaging to 13.7 channels per isotope. Per isotope, each channel has a different alpha particle energy that corresponds to the population of the relevant daughter nucleus level. Additionally, a probability of occurrence has been assigned to each reaction channel based on data from the DDEP database [6]. Figure 1 illustrates the α-spectra of [232]Th, [242]Pu, [241]Am and [252]Cf. Although in this particular case the spectra are separated, in general they can overlap.

The main parameter that determines the alpha particle yield is the α-decay half-life. It ranges from 163 days for [242]Cm to $1.40 \cdot 10^{10}$ years for [232]Th, resulting to the difference of α-particle and neutron yields by more than 11 orders of magnitude [6]. The Table 1 gives the total half-life for the isotopes of interest from the old reference [1] and updated values extracted from the ENSDF and DDEP databases. The alpha energies and branching ratios are also taken from the DDEP database. When data from both databases was available, preference was given to DDEP.
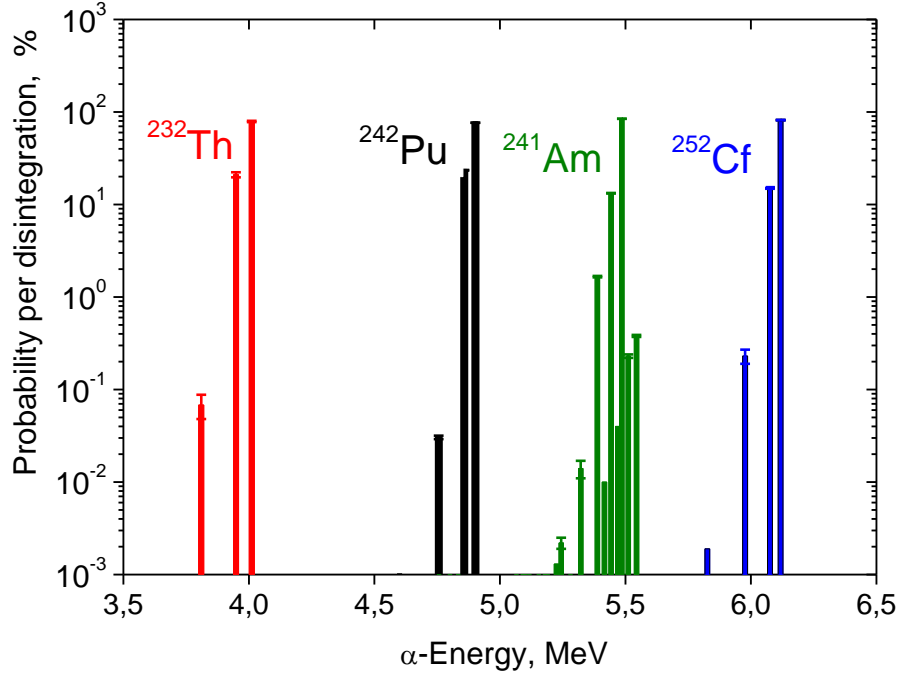
Fig 1. Alpha radiation emission spectra resulting from spontaneous α-decay of [232]Th, [242]Pu, [241]Am and [252]Cf isotopes [6]. Each decay channel has its own energy and probability of occurring.

Table 1. Total half-life times used in Report NUREG/CR-5550 [1] (OLD) and present revision (NEW) including uncertainties (u).

Isotope	Total T1/2 OLD, s	Total T1/2 NEW, s	u(T1/2), s	Database	% change
Am-241	1.368E+10	1.365E+10	1.893E+07	DDEP	-0.23
Bk-249	2.765E+07	2.850E+07	1.261E+08	ENSDF	3.08
Cf-252	8.618E+07	8.353E+07	8.205E+04	DDEP	-3.08
Cm-242	1.408E+07	1.407E+07	6.912E+03	DDEP	-0.09
Cm-244	5.712E+08	5.715E+08	9.467E+05	DDEP	0.06
Np-237	6.753E+13	6.766E+13	2.209E+11	DDEP	0.19
Pu-238	2.769E+09	2.769E+09	9.467E+05	DDEP	0
Pu-239	7.605E+11	7.605E+11	3.471E+08	DDEP	0
Pu-240	2.070E+11	2.070E+11	2.209E+08	DDEP	0.02
Pu-241	4.529E+08	4.522E+08	1.262E+06	DDEP	-0.14
Pu-242	1.187E+13	1.177E+13	9.467E+10	DDEP	-0.80
Th-232	4.450E+17	4.424E+17	1.893E+15	DDEP	-0.57
U-232	2.263E+09	2.228E+09	3.471E+07	DDEP	-1.53
U-233	5.018E+12	5.020E+12	6.307E+09	DDEP	0.05
U-234	7.732E+12	7.747E+12	1.893E+10	ENSDF	0.20
U-235	2.222E+16	2.222E+16	3.156E+13	DDEP	0
U-236	7.384E+14	7.394E+14	1.893E+12	DDEP	0.13
U-238	1.411E+17	1.410E+17	1.578E+14	DDEP	-0.04

For the most isotopes, the changes of half-lifes are less than 1%, for several others – up to 3%. These changes have direct (inversely proportional) impact on the isotope specific α-particle rate and, therefore, on the resulting neutron yield.

Note that the total half-life is given rather than the α-decay time. For most of these isotopes, they are equal except for isotopes with decay modes other than α-emission. This is taken into account through the branching fractions which are defined relative to the total probability of decay modes. Hence, the sum of all alpha decay branching fractions for isotopes with multiple decay modes could be smaller than 1.

From the information in Table 1, together with atomic mass data, the alpha yields can be computed for each actinide. The alpha yield data is given in Table 2. The neutron yield is linearly dependent on the alpha yield, although in this revision the full decay spectra are used rather than an average alpha energy.

Table 2. Isotope decay and alpha yield data with uncertainties (u) and source of origination.

Isotope	Total T1/2, s	u(T1/2), s	α-yield α/s·g	u(α-yield) %	Average α-energy, MeV	Database
Am-241	1.365E+10	1.893E+07	1.268E+11	0.14	5.479	DDEP
Bk-249	2.850E+07	1.829E+03	8.526E+08	0.01	5.406	ENSDF
Cf-252	8.353E+07	8.205E+04	1.982E+13	0.10	6.111	DDEP
Cm-242	1.407E+07	6.912E+03	1.226E+14	0.05	6.101	DDEP
Cm-244	5.715E+08	9.467E+05	2.993E+12	0.17	5.795	DDEP
Np-237	6.766E+13	2.209E+11	2.603E+07	0.33	4.768	DDEP
Pu-238	2.769E+09	9.467E+05	6.333E+11	0.03	5.487	DDEP
Pu-239	7.605E+11	3.471E+08	2.296E+09	0.05	5.148	DDEP
Pu-240	2.070E+11	2.209E+08	8.398E+09	0.11	5.156	DDEP
Pu-241	4.522E+08	1.262E+06	9.317E+07	0.28	4.894	DDEP
Pu-242	1.177E+13	9.467E+10	1.465E+08	0.80	4.892	DDEP
Th-232	4.424E+17	1.893E+15	4.066E+03	0.43	3.998	DDEP
U-232	2.228E+09	3.471E+07	8.074E+11	1.56	5.302	DDEP
U-233	5.020E+12	6.307E+09	3.568E+08	0.13	4.817	DDEP
U-234	7.747E+12	1.893E+10	2.302E+08	0.24	4.759	ENSDF
U-235	2.222E+16	3.156E+13	7.994E+04	0.14	4.391	DDEP
U-236	7.394E+14	1.893E+12	2.392E+06	0.26	4.481	DDEP
U-238	1.410E+17	1.578E+14	1.244E+04	0.11	4.187	DDEP

Since the previous revision of neutron yields, not only the adopted decay times have changed, but also their uncertainties have decreased. This allows for more accurate determination of the neutron yield.

3.2 Basic Nuclear Cross Sections

The fuel materials considered here are UO_2, UF_6, PuO_2 and PuF_4. At aforementioned alpha energies, any U(α,xn) or Pu(α,xn) reactions are practically prohibited due to the threshold which lies above 11 MeV. Therefore, we need to focus on the (α,xn) reactions with naturally occurring on the oxygen and fluorine isotopes only.

For natural oxygen and fluorine, we present the isotopic neutron producing microscopic cross sections which we used for the neutron yield calculations. The required evaluated cross section data for the reactions $^{17}O(α,xn)$, $^{18}O(α,xn)$ and $^{19}F(α,xn)$ was searched in the following libraries:

- JENDL/AN-2005 [3],   retrieved from https://www-nds.iaea.org/exfor/endf.htm ;
- ENDF/B-VII.1 [5],   retrieved from https://www-nds.iaea.org/exfor/endf.htm ;
- TENDL-2014 [8],   retrieved from http://www.talys.eu/tendl-2014/ ;
- JEFF-3.2 [9],   retrieved from https://www-nds.iaea.org/exfor/endf.htm .

The data for the reaction reactions of interest are not available in the JEFF-3.2 or ENDF/B-VII.1 libraries. The data, we found and presented below, are pointwise data at 293 K which allow lin-lin interpolation between points.

The experimental data were searched in EXFOR.

3.2.1. $^{17}O(\alpha,xn)$ Reaction

Evaluated cross section data:

Library	Max E_α [MeV]	No. of Data points
TENDL-2014	200	45
JENDL/AN-2005	15	373

In order to evaluate which reaction channels are of interest, the (α,xn) reactions that occur at energies below 20 MeV are provided:

Reaction	Q-value [MeV]	Threshold [MeV]
$^{17}O(\alpha,n)\,^{20}Ne$	0.5867	0.0000
$^{17}O(\alpha,\alpha'n)\,^{16}O$	-4.1429	5.1184
$^{17}O(\alpha,pn)\,^{19}F$	-11.7453	14.5108
$^{17}O(\alpha,2n)\,^{19}Ne$	-16.2779	20.1107

From these data we can conclude that only the (α,n) and $(\alpha,\alpha'n)$ reaction can occur, among them (α,n) has the largest contribution to the neutron yield.

The evaluated data are presented together with experimental data in Fig. 2 from Bair (1973) [10] and Hansen (1967) [11]. As stated by the authors, data from Bair and Hansen comes with an estimated ±7% and ±10% error margin.
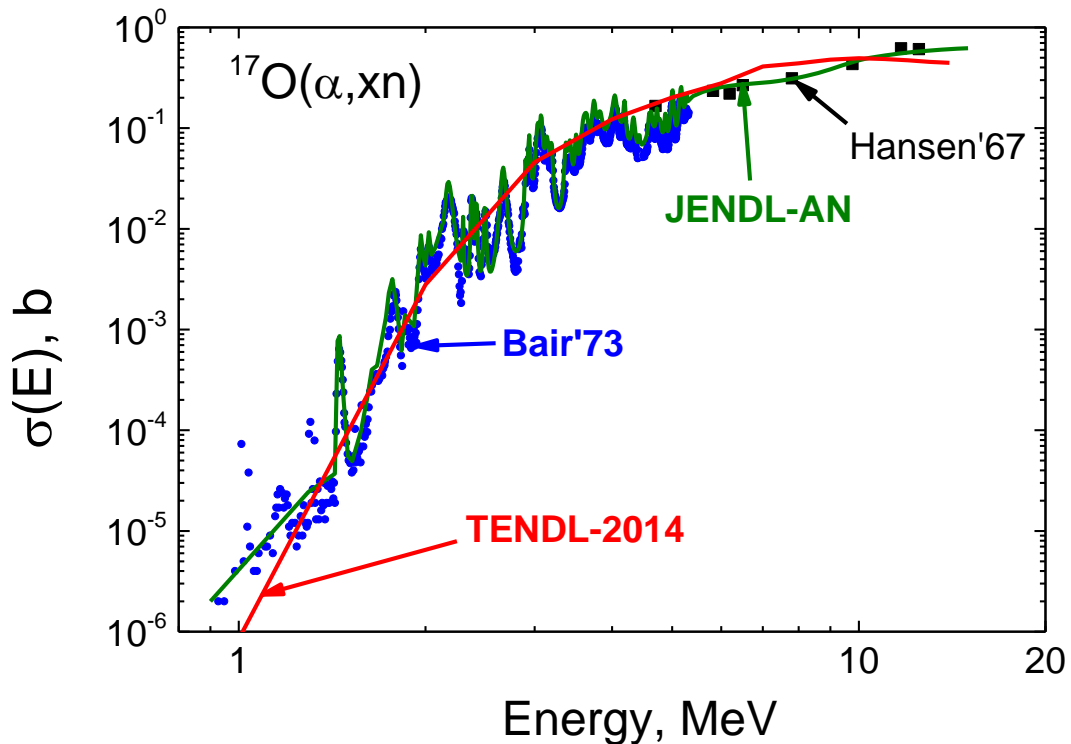
Fig 2. Total neutron production cross section resulting from the $^{17}O(\alpha,xn)$ reaction: evaluations – JENDL/AN [3] and TENDL-2014 [8]; experimental data – Bair [10], Hansen [11].

3.2.2. ^{18}O(α,xn) Reaction

Evaluated cross section data:

Library	Max E_α [MeV]	No. of Data points
TENDL-2014	200	45
JENDL/AN-2005	15	314

In order to evaluate which reaction channels are of interest, the (α,xn) reactions that occur at energies below 17 MeV are provided:

Reaction	Q-value [MeV]	Threshold [MeV]
^{18}O(α,n) ^{21}Ne	-0.6974	0.8525
^{18}O(α,2n) ^{20}Ne	-7.4583	9.1169
^{18}O(α,α'n) ^{17}O	-8.0451	9.8341
^{18}O(α,pn) ^{20}F	-13.1893	16.1222

From this data we can conclude that only the (α,n) reaction channel is accessible for the alpha-particle energy range of interest.

The evaluated data are presented together with experimental data in Fig. 4 from Bair (1962, 1973) [12,10] and Hansen (1967) [11]. As stated by the authors, data from Bair and Hansen come with an estimated uncertainties ±7% and ±10%. Although the two datasets from Bair are consistent in the range of overlap, data from Bair (1973) have not been considered in the JENDL/AN-2005 evaluation. Therefore, the resonant structure is not reflected in JENDL/AN and no good agreement with experimental data can be observed for alpha energies lower than 2.5 MeV.
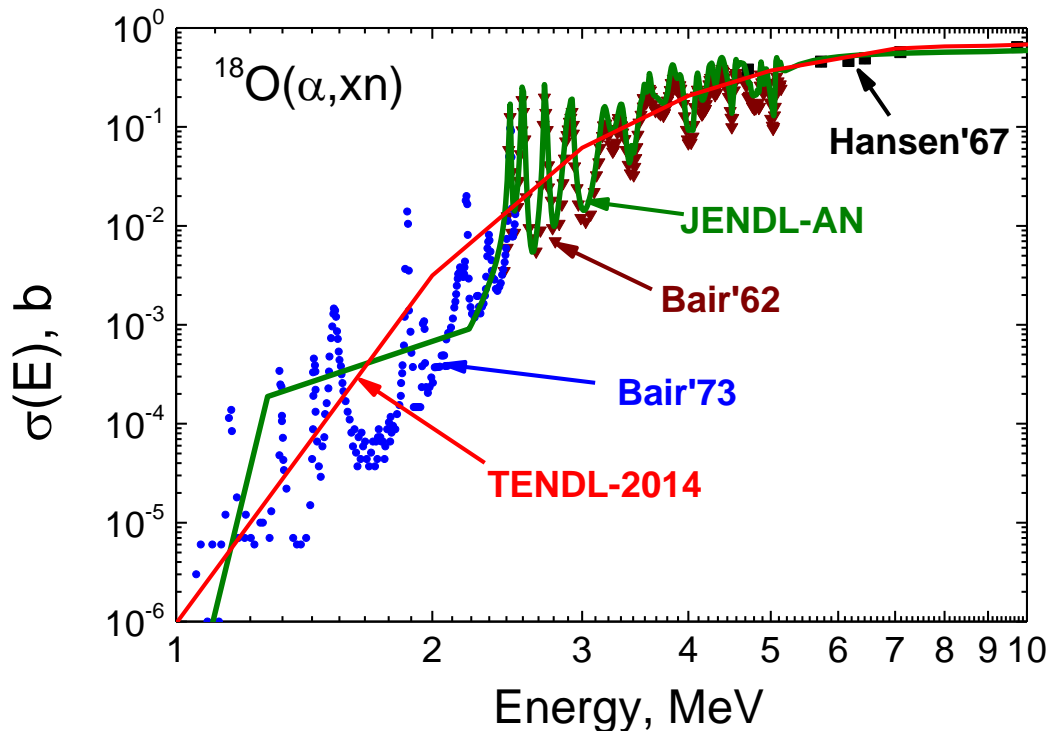
Fig 3. Total neutron production cross section resulting from the ^{18}O(α,xn) reaction: evaluations – JENDL/AN [3] and TENDL-2014 [8]; experimental data – Bair [10,12] and Hansen [11].

3.2.3. ^{19}F(α,xn) Reaction

Evaluated cross section data:

Library	Max E$_α$ [MeV]	Data points
TENDL-2014	200	45
JENDL/AN-2005	15	56

In order to evaluate which reaction channels are of interest, the(α,xn) reactions that occur at energies below 16 MeV are provided:

Reaction	Q-value [MeV]	Threshold [MeV]
^{19}F(α,n) ^{22}Na	-1.9523	2.3636
^{19}F(α,pn) ^{21}Ne	-8.1798	9.9031
^{19}F(α,α'n) ^{18}F	-10.4315	12.6292
^{19}F(α,2n) ^{21}Na	-13.0201	15.7631

From this data we can conclude that only the (α,n) reaction channel is accessible for the alpha-particle energy range of interest. For the ^{19}F(α,xn) reaction the data are available from P. Wrean [13] (2.3 < E$_α$ < 3.1 MeV) and E. Norman [14] (3.6 < E$_α$ < 9.9 MeV, however the cross sections were derived from the thick target yield) with an estimated uncertainty of 10%. The energy grid and measurement uncertainties are not fine enough to be able to account for the resonant structure of the cross section. Therefore, no evaluated data is available that considers the resonant structure.
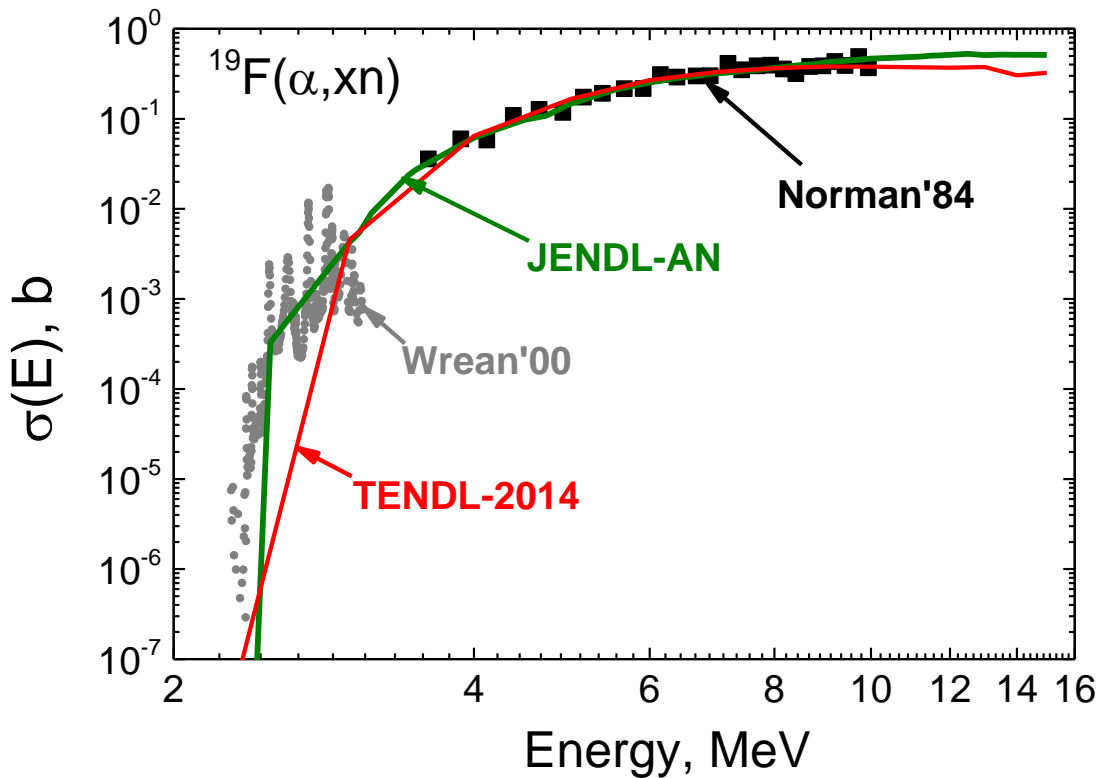
Fig 4. Total neutron production cross section resulting from the ^{19}F(α,xn) reaction: evaluations - JENDL/AN [3], TENDL-2014 [8]; experimental data - Wrean [13] and Norman [14].

3.2.4. Discussion

JENDL/AN data [3] have been evaluated in such a way that they reproduce the resonance structure determined experimentally by Bair et al. for ^{17}O [10] and ^{18}O [12]. However, Bair' data [10] were not considered in the JENDL/AN evaluation for ^{18}O, even though they were available at the time of evaluation. The experimental $^{18}O(\alpha,n)$ cross sections published by Bair and Willard in 1962 [12] have been multiplied by a corrective factor of 1.35 as proposed by authors later in 1979 [7].

JENDL/AN and TENDL evaluations do not consider the resonance structure of the neutron production cross section for ^{19}F as stated by the JENDL/AN authors on p. 46 of [3]. However, the resonance structure is visible in experimental data presented by Wrean in the incident energy range between 1 and 3 MeV [13]. The measurement of Norman in the energy range from 4 to 10 MeV shows smooth behaviour.

3.3 Stopping power

The alpha particles emitted by the heavy isotopes of interest are stopped in reactor fuel materials, of which we consider uranium dioxide (UO_2), plutonium fluoride (PuF_4) and uranium fluoride (UF_6). The SRIM [4] and ASTAR [15] codes are available to compute stopping powers for alpha particles incident on any element up to uranium. For the relevant elements, their results differ by less than 5% for incident alpha particle energies above 1 MeV as demonstrated with the example of an oxygen target. Below this value, there is a discrepancy of no more than 18%, however, the neutron production cross sections in this range are small.

We used the SRIM code [4] to compute the mass stopping power of alpha particles in pure uranium, oxygen and fluorine in the range of 0 to 20 MeV. We then calculate the stopping power for compounds by linearly summing the contributions of each constituent component in accordance with the Brag-Kleeman rule [16, p. 43]. In this linear summation, the weights represent the mass fraction of the respective atom presented in the compound.

To illustrate this concept, the linear stopping powers of uranium, oxygen and its compound uranium dioxide are plotted in Fig. 5 at a typical solid density of 10.97 g/cm^3. For this example, the UO_2 stopping power was directly calculated by the SRIM code. Uranium being the more massive element has a higher stopping power than a lighter element such as oxygen. As expected, uranium dioxide has a stopping power that lies in between of ones for U and O.
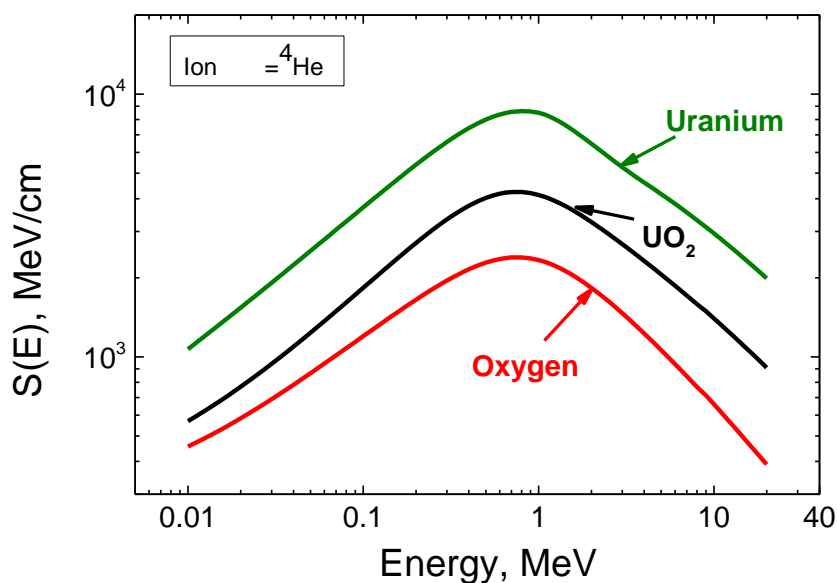
Fig 5. Stopping power for uranium, solid oxygen and its compound UO_2 at typical densities computed with the SRIM code [4].

In comparison to the neutron production cross sections, the stopping power is a smooth function. For subsequent calculations that require an equal energy grid for the cross sections and stopping power, the stopping power will be interpolated for this reason rather than the cross sections which have a complex resonance structure.

The stopping power can also be used to compute an average projected range Δx of alpha particles in the reactor fuel materials. This can be done with the equation:

$$\Delta x = \int_0^{E_\alpha} \frac{1}{S(E)}\, dE,$$

where S(E) represent the linear stopping power. SRIM results for UO_2 reveal that this range is below of 50 μm for incident energies up to 10 MeV, with the range being comparable in all other stopping media. Any container holding reactor fuel material has much larger typical dimensions, justifying the infinitely thick target approximation.

The stopping power for plutonium is not tabulated, nor can it be computed with the SRIM code. A scaling approach was used where the electronic component of the stopping power is scaled according to the nuclear charge, as it appears in Bethe's formula [16]. The nuclear stopping power is assumed to be the same as that of uranium.

3.4 Mass densities

Where atomic densities are needed, such as in the yield equation, standard atmospheric conditions are assumed (p = 1 bar, T= 293 K). The resulting densities of reactor fuel materials which follow from these conditions and are assumed in this report are:

Fuel	Molar mass g/mol	Density g/cm^3
UO_2	270.030	10.970
UF_6	351.990	5.090
PuF_4	319.890	7.100
PuO_2	276.000	11.500

Whereas fluorine has only one naturally occurring isotope, ^{19}F, oxygen has three. The oxygen isotope composition of oxide fuels was taken to be equal to the natural oxygen abundance as currently recorded in the ENDF database:

Isotope	^{16}O	^{17}O	^{18}O
Abundance, %	99.757	0.038	0.205

These abundance figures were used to compute the partial densities of each target isotope (oxygen and fluorine) in the fuel material to be used in the yield equation (it appears as N_T). For each reactor fuel indicated in the upper left corner, the partial densities used in our revision are as listed in the following tables.

For oxide fuels:

UO_2	Partial density, g/cm^3
^{16}O	1.296
^{17}O	$5.2485 \cdot 10^{-4}$
^{18}O	$2.9980 \cdot 10^{-3}$

PuO_2	Partial density, g/cm^3
^{16}O	1.330
^{17}O	$5.3830 \cdot 10^{-4}$
^{18}O	$3.0748 \cdot 10^{-3}$

For fluoride fuels:

UF$_6$	Partial density, g/cm^3
^{19}F	1.648

PuF$_4$	Partial density, g/cm^3
^{19}F	1.687

4. Code validation

The Fortran 90 code used in this work was validated using experimental data of thick targets (α,xn) neutron yields from Bair [7], West [17] and Jakobs [18]. The experimental data from Bair have an approximate uncertainty 10%, which is larger than ones from West (< 2%) and from Jakobs (< 5%), the precise values are given in their corresponding EXFOR entries.
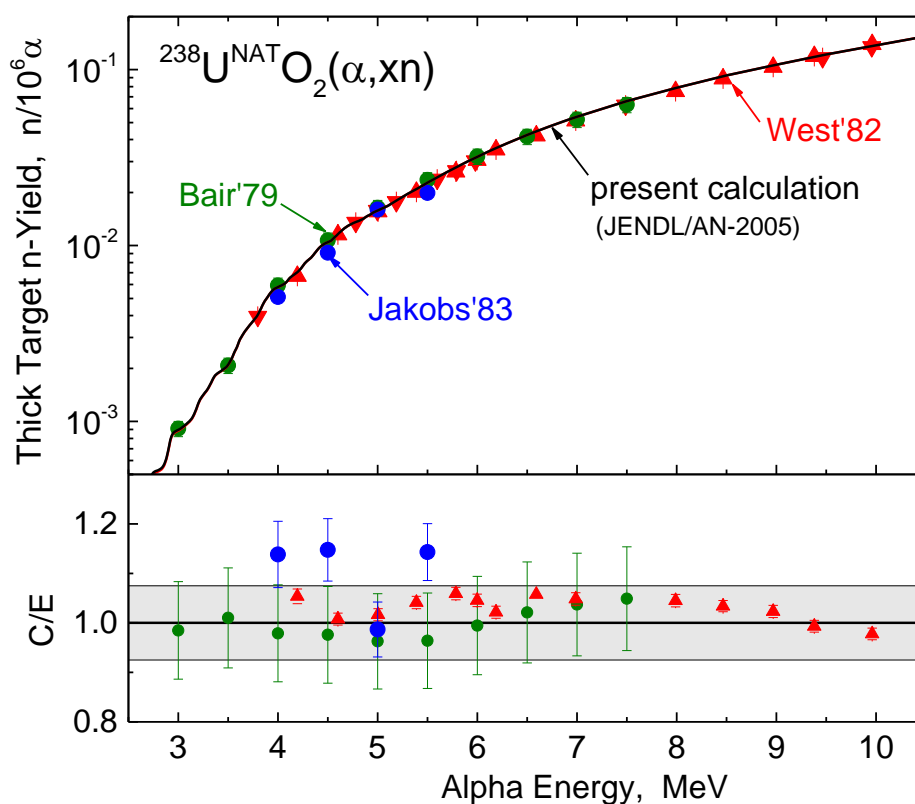
Fig 6. Tick target neutron yield from alpha particles incident on a UO$_2$ target. The yield calculated by the developed Fortran code is compared with measured data of Bair [7], West [17] and Jakobs [18].

Fig. 6 is considered as a benchmark for the code and input data. The C/E ratios, the calculated over the experimental yield, were computed for each experimental data point. In the ideal case with perfect agreement, this ratio equals unity. The grey band denotes the uncertainty range of the ratio where the uncertainty follows only from uncertainty in the calculation (as a direct result from uncertainty in the cross section, stopping power and other input data). Each experimental point is plotted with its corresponding experimental uncertainty and the two ranges show overlap for every point, indicating agreement between this UO$_2$ yield calculation and experiments. Therefore, the code and data used are now considered as reliable for the yield calculations for other reactions of interest.

5. (α,n) Neutron yield results for fuel materials

This section will present the neutron yield results for each actinide in the fuel material in which they occur. The calculations performed make use of the neutron yield equation described in Section 2, as well as the input data from previous sections.

All data are presented with uncertainties which originate from uncertainty in the input data. For the following results, the uncertainty in the neutron yield is calculated from the uncertainty of all the input data using a linearised propagation of uncertainty scheme. The parameters which determine the neutron yield uncertainty are the alpha energies, the branching fractions, half-life, stopping power and neutron production cross sections. The uncertainties in these parameters are treated as independent.

For the neutron production cross sections, the uncertainty as specified by each respective author is considered to be fully correlated as they originate partly from an overall normalization factor. Despite the fact that cross section data have several hundreds of data points, the averaged cross section uncertainty does not drop to very low value. This worst case assumption was made because no knowledge of the correlation matrix is present.

5.1 Neutron yield in UO_2

Neutron yields for actinides embedded in uranium dioxide are given in Table 3. For uranium dioxide, the uncertainty of the (α,n) cross sections makes up the largest contribution to the yield uncertainty with a systematic uncertainty of 7% [10]. The stopping power uncertainty which is treated as a statistical uncertainty, is 6% for alpha particles in UO_2.

Table 3. Old ([1]) and New (present work with uncertainty u) neutron yields and their Ratio for actinides embedded in UO_2. The ratios different from unity by two standard deviations are highlighted in red.

Isotope	Old n-yield n/s·g	New n-yield n/s·g	u(New n-yield) %	Yield Ratio New/Old
Am-241	2.69 E+03	2.837 E+03	7.13	1.055
Bk-249	1.80 E+01	1.806 E+01	7.13	1.003
Cf-252	6.00 E+05	6.773 E+05	7.13	1.129
Cm-242	3.76 E+06	4.163 E+06	7.13	1.107
Cm-244	7.73 E+04	8.359 E+04	7.14	1.081
Np-237	3.40 E-01	3.498 E-01	7.14	1.029
Th-232	2.20 E-05	2.483 E-05	7.22	1.129
U-232	1.49 E+04	1.589 E+04	7.30	1.064
U-233	4.8	4.936	7.14	1.028
U-234	3.0	3.085	7.13	1.028
U-235	7.10 E-04	7.473 E-04	7.13	1.053
U-236	2.40 E-02	2.463 E-02	7.80	1.026
U-238	8.30 E-05	8.705 E-05	7.14	1.049

The ratio indicates how much the newly calculated neutron yields differ from the previously accepted values. In most cases, the newly evaluated yields agree within one uncertainty margin with the previous reference values.

5.2 Neutron yield in UF_6

Neutron yields for uranium isotopes embedded in uranium hexafluoride are given in Table 4. The relevant neutron production cross section for UF_6 is that of ^{19}F, which has a higher uncertainty

estimated by Wrean to be 10% [13]. The second largest source of uncertainty stems from the stopping power which is 4.9% as specified by the authors of the SRIM code [4]. Here the uncertainty in the stopping power is treated being statistical by nature.

Table 4. Old ([1]) and New (present work including uncertainty u) neutron yield results for uranium isotopes embedded in **UF$_6$**. The ratios different from unity by two standard deviations are highlighted in red.

Isotope	Old n-yield n/s·g	New n-yield n/s·g	u(n-yield) %	Yield ratio New/Old
U-232	2.60 E+06	3.809 E+06	10.2	1.465
U-233	7.00 E+02	9.252 E+02	10.1	1.322
U-234	5.80 E+02	5.519 E+02	10.1	0.952
U-235	8.00 E-02	1.162 E-01	10.1	1.453
U-236	2.90 E+00	3.930 E+00	10.5	1.355
U-238	2.80 E-02	1.257 E-02	10.1	0.449

The newly calculated neutron yields in UF$_6$ appear to differ significantly from the previously accepted yields by several uncertainty margins, except the case of isotope ^{234}U. Such a deviation cannot be explained by a change in the decay data, as the same uranium isotopes are considered as for the case of UO$_2$. Also the stopping power data for UF$_6$ have not changed since [1] appeared. The deviations in the newly calculated neutron yields can be attributed primarily to the revision of the cross section data for ^{19}F, since the experimental data of Wrean [13] were published in the year 2000 or after issue of Report NUREG/CR-5550 [1] in 1991.

5.3 Neutron yield in PuO$_2$

Neutron yields for plutonium isotopes embedded in plutonium dioxide are given in Table 5. The uncertainty in cross section has the largest contribution to the neutron yield uncertainty. It is determined by the neutron production cross sections of natural oxygen isotopes and set at 7% as specified by the original authors [10]. The stopping power was estimated to have an uncertainty of 6%, identical to that of UO$_2$ from which it was derived through scaling of the nuclear charge following the Bethe's equation and assuming an equal nuclear stopping power.

Table 5. Old ([1]) and New (present work including uncertainty u) neutron yields and their Ratio for plutonium isotopes embedded in **PuO$_2$.** The ratios different from unity by two standard deviations are highlighted in red.

Isotope	Old n-yield n/s·g	New n-yield n/s·g	u(New n-yield) %	Yield ratio New/Old
Pu-238	1.34 E+04	1.381 E+04	7.13	1.030
Pu-239	3.81 E+01	3.883 E+01	7.13	1.019
Pu-240	1.41 E+02	1.429 E+02	7.13	1.013
Pu-241	1.30	1.322	7.14	1.018
Pu-242	2.00	2.205	7.17	1.102

The revised neutron yields for plutonium isotopes in oxide fuel are close to their old values in the most cases.

5.4 Neutron yield in PuF₄

Neutron yields for plutonium isotopes embedded in plutonium tetrafluoride are given in Table 6. The relevant neutron production cross section for UF_6 is that of ^{19}F, which has an uncertainty estimated by Wrean to be 10% [13]. The second largest source of uncertainty stems from the stopping power which is 5.2%. The stopping power and its uncertainty are derived from the stopping power of fluoride and the scaled stopping power of uranium. Scaling was done by scaling the nuclear charge in Bethe's equation and assuming an equal nuclear stopping power.

Table 6. Old ([1]) and New (present work including uncertainty u) neutron yields and their Ratio for plutonium isotopes embedded in **PuF₄**. The ratios different from unity by two standard deviations are highlighted in red.

Isotope	Old n-yield n/s·g	New n-yield n/s·g	u(New n-yield) %	Yield ratio New/Old
Pu-238	2.20 E+06	2.875 E+06	10.05	1.307
Pu-239	5.60 E+03	7.278 E+03	10.05	1.300
Pu-240	2.10 E+04	2.688 E+04	10.05	1.280
Pu-241	1.70 E+02	2.148 E+02	10.06	1.263
Pu-242	2.70 E+02	3.368 E+02	10.05	1.247

Similarly to neutron yields in UF_6 there is an increase of the new neutron yields for plutonium isotopes in fluoride of plutonium,. The main cause of this is the recently revised cross section data of ^{19}F [3]. This deviation grows larger than for the case of UF_6 because the plutonium isotopes emit alpha particles with higher energies. The average alpha energies for plutonium isotopes are around 0.5 MeV higher than those for the uranium isotopes, see Table 2.

6. Conclusion and requests for new measurements and evaluations

For the neutron production cross section on ^{18}O, the JENDL/AN evaluation did not consider the resonance structure observed in measurements of Bair (1973) [10] in the energy range below 2.5 MeV, even though they were available at the time of the evaluation. In this range, the evaluated data reproduce the oscillating experimental data only in average.

Thus we recommend to include the resonance structure in the next evaluation release. It worthwhile to note that such resonant structure in the $^{18}O(\alpha,xn)^{21}Ne$ and $^{17}O(\alpha,xn)^{20}Ne$ excitation functions below 5 MeV was analysed by the R-matrix theory and parametrized by the SAMMY code [19].

In general, the specific neutron yields produced by the α-decaying actinide isotopes in the uranium and plutonium oxides. UO_2 and PuO_2, do agree with the previous reference data [1] within 1.0-1.5 uncertainties or (7-12)% assigned to the present calculations.

The largest deviations ($\approx$ 25 - 50%) from the previous reference values [1] were found for the neutron yields from actinides embedded in both fluorides UF_6 and PuF_4. The main reason of such changes is the use of the new cross section for the $^{19}F(\alpha,xn)$ reaction from JENDL/AN-2005, which took into account the experimental data of Norman [14] and Wrean [13] appeared after release of the reference evaluations [1,2] in 1991. However, the JENDL/AN-2005 evaluated cross section for ^{19}F ignored strong resonance structure which was experimentally observed for $^{19}F(\alpha,xn)$ reaction below 5 MeV.

The other reason which could contribute to the discrepancies is the stopping power of α-particles in Pu. We derived it by scaling of U data using the nuclear charge ratio, there are no experimental data to prove it.

During this study we found several articles which reports the (α,xn) or (α,xγ) cross sections measurements [20-24] but still missed in EXFOR (NDS of IAEA has assigned them for compilation).

It is also worth to mention that there are efforts underway now to measure the (α,n) cross sections for ^{19}F in the range between 3 and 6 MeV [25]. The new experimental data with energy resolution sufficient to uncover the resonance structure will significantly improve the reliability of the neutron yields computing in fuel materials containing fluorine.

One of the key data inputs for neutron yield calculations is the stopping powers, which are not available for pure plutonium or compounds containing its large fraction. Without such data an element-to-element scaling approximation has to be used without experimental verification. To improve the reliability of neutron yields calculations, the stopping power of α-particles in Pu, PuF_4 and PuO_2 have to be measured in the energy range below 6 MeV.

Acknowledgments

References

1. D. Reilly, N. Ensslin and H. Smith, *Passive Nondestructive Assay of Nuclear Materials*, Report NUREG/CR-5550, Los Alamos Laboratory, 1991

2. R.T. Perry and W.B. Wilson, *Neutron Production from (α,n) Reactions and Spontaneous Fission in ThO$_2$, UO$_2$, and (U,Pu)O$_2$ Fuels*, Report LA-8869-MS Los Alamos National Laboratory, 1981

3. T. Murata, H. Matsunobu and K. Shibata, *Evaluation of the (a,xn) Reaction Data for JENDL/AN-2005*, Report JAEA-Research 2006-052, JAERI, 2006

4. J.F. Ziegler, *The Stopping of Energetic Light Ions in Elemental Matter,* J. Appl. Phys./Rev. Appl. Phys. 85 (1999) 1249

5. M.B. Chadwick, M. Herman et al., *ENDF/B-VII.1 Nuclear Data for Science and Technology: Cross Sections, Covariances, Fission Product Yields and Decay Data*, Nucl. Data Sheets 112 (2011) 2887

6. A. Arinc et al., *Decay Data Evaluation Project,* www.nucleide.org/DDEP.htm (2014). Accessed 10-10-2015

7. J.K. Bair and J. Gomez del Campo, *Neutron Yields from Alpha-Particle Bombardment,* Nuclear Science and Engineering 71 (1979) 18, EXFOR C0595009

8. A.J. Koning and D. Rochman, *TENDL-2014: Consistent TALYS-based Evaluated Nuclear Data Library including Covariance data* (2014) ftp://ftp.nrg.eu/pub/www/talys/tendl2014/tendl2014.html

9. A. Koning, R. Forrest et al., *The JEFF-3.1 Nuclear Data Library* (2006), ISBN 92-64-02314-3

10. J.K. Bair and F.X. Haas, *Total neutron yield from the reactions $^{13}C(a,n)^{16}O$ and $^{17,18}O(a,n)^{20,21}Ne$,* Physical Review C7(1973)11356, EXFOR C0489, C1010

11. L.F. Hansen, J.D. Anderson, et al., *The (α,n) cross sections on ^{17}O and ^{18}O between 5 and 12.5 MeV*, Nuclear Physics A98 (1967) 25, EXFOR P0116

12. J.K. Bair and H.B. Willard, *Level Structure in ^{22}Ne and ^{30}Si from the Reactions $^{18}O(α,n)^{21}Ne$ and $^{26}Mg(α,n)^{29}Si$,* Phys. Rev. 128 (1962) 299, EXFOR P0120002

13. P.R. Wrean and R.W. Kavanagh, *Total cross sections and reaction rates for 19F(a,n)22Na and 22Ne(p,n)22Na and their inverses,* Physical Review C62 (2000) 055805, EXFOR C1049002

14. E.B. Norman, T.E. Chupp et al., *^{22}Na production cross sections from the $^{19}F(α,n)$ reaction*, Phys. Rev. C30(1984)1339, EXFOR C1433002

15. ICRU (1993). International Commission on Radiation Units and Measurements. *ICRU Report 49*, *Stopping Powers and Ranges for Protons and Alpha Particles*

16. G.F. Knoll, *Radiation detection and measurement*, 2nd edition, John Wiley and Sons, New York (1989)

17. D. West and A.C. Sherwood, *Measurements of thick-target (α,n) yields from light elements, A*nn. Nucl. Energy 9(1982)551, EXFOR D0048

18. G.J.H. Jakobs and H. Liskien, *Energy Spectra of Neutrons produced by α-particles in Thick Targets of Light Elements*, Annals of Nuclear Energy 10(1983)541, EXFOR F0341007

19. R. Babut, O. Bouland and E. Fort, *Reich-Moore Parameterization of (a,n) Reactions on Light Nuclei: Impact on a Neutron Source Calculation in an Oxide Fuel*, NSE 151(2005) 135

20. L. van der Zwan and K.W. Geiger, Energy Levels in ^{23}Na from the $^{19}F(α,n)^{22}Na$ reaction, Nucl. Phys. A284(1977)189

21. M. Balakrishnan, S. Kailas and M.K Mehta, *A study of the reaction $^{19}F(α,n)^{22}Na$ in the bombarding energy range 2.6 to 5.1 MeV*, Pramina 10(1978)329

22. E.B. Norman, K.T. Lesko, T.E. Chupp et al., *Gamma-Ray Production Cross Sections for Alpha-Particle Induced Reactions on ^{19}F and ^{23}Na*, Radiation Effects 94(1986)307

23. A. Denker, Drei Neutronenerzeugungsreaktionen in Sternen, Dissertation, Universität Stuttgart, 1994, Verlag Shaker, Aachen, ISBN 3-8265-0191-8

24. R. Kunz, A. Denker, H.W. Drotleff et al., Neutron sources in nuclear astrophysics, International Conference on Neutrons and their Applications, Proc. of SPIE 2339(1995)38

25. W. Peters, M. Smith et al.*, A Kinematically Complete, Interdisciplinary, and Co-Institutional Measuring of the $^{19}F(α,n)$Cross Section for Nuclear Safeguards*, http://www.osti.gov/scitech/biblio/1154645/